ACS APPLIED MATERIALS & INTERFACES

www.acsami.org

Research Article

Neutralizing Defect States in MoS_2 Monolayers

Xiaheng Huang,[‖] Zidong Li,[‖] Xiao Liu, Jize Hou, Jongchan Kim, Stephen R. Forrest, and Parag B. Deotare*

Cite This: *ACS Appl. Mater. Interfaces* 2021, 13, 44686−44692

Read Online

ACCESS | Metrics & More | Article Recommendations | Supporting Information

ABSTRACT: We report a method to neutralize the mid-gap defect states in MoS_2 monolayers using laser soaking of an organic/transition metal oxide (TMO) blend thin film. The treated MoS_2 monolayer shows negligible emission from defect states as compared to the as-exfoliated MoS_2, accompanied by a photoluminescence quantum yield improvement from 0.018 to 4.5% at excitation power densities of 10 W/cm^2. The effectiveness of the method toward defect neutralization is governed by the polaron pair generated at the organic/TMO interface, the diffusion of free electrons, and the subsequent formation of TMO radicals at the MoS_2 monolayer. The treated monolayers are stable in air, vacuum, and acetone environments, potentially enabling the fabrication of defect-free optoelectronic devices based on 2D materials and 2D/organic heterojunctions.

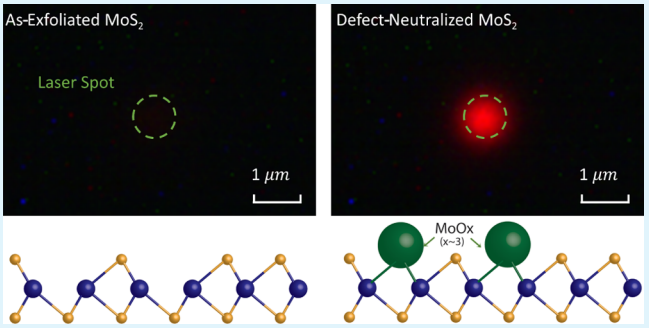

KEYWORDS: *transition metal dichalcogenides, organic/transition metal oxide, defect neutralization, photoluminescence quantum yield, laser soaking*

INTRODUCTION

Wafer-scale transition metal dichalcogenide (TMD) monolayers[1−4] offer an emerging platform for next-generation optoelectronic devices.[5−11] However, realization of practical devices has been hindered by the intrinsic and extrinsic surface defects[12−17] present in the material system that results in extremely low (∼0.01%) photoluminescence quantum yield (PLQY).[10,18,19] Several methods[19−26] based on chemical[21,22,24] or physical[20,23] treatments have been proposed in recent years to enhance the PL of monolayer TMDs. The most notable approach is using "superacid" (bis-(trifluoromethane) sulfonimide, TFSI) for surface treatment that leads to near-unity PLQY of MoS_2.[19] The superacid serves as a Lewis acid (i.e., electron pair acceptor) that suppresses the formation of charged excitons (trions).[20] Trions are nonexistent in the pristine material and hence their elimination is regarded as the underlying mechanism for PL enhancement of TMDs.[20,25,27−31] However, the PL enhancement in the case of TFSI does not originate from the elimination of intrinsic defect states as it has been shown that the native defect states are preserved[20,32] after such treatment. On the other hand, various approaches for passivation of defects have been reported but with limited success. None of the reported work quantifies the PLQY or show complete elimination of defect states.[24,27,28,33−35]

Here, we report a method and underlying physics of treating mechanically exfoliated monolayer MoS_2 using an organic/transition metal oxide (TMO) blend under laser excitation (light soaking). We directly verify the elimination of defect states commonly associated with sulfur vacancies by the disappearance of their luminescent spectral signature. For an optimum blend ratio of 20%:80% (vol) 3,3′,5,5′-tetra[(*m*-pyridyl)-phen-3-yl]biphenyl (BP4mPy)/MoO_x, the PL intensity of a treated MoS_2 monolayer is enhanced by ∼250 times when compared to the as-exfoliated MoS_2. The PLQY reaches ∼4.5% at an excitation power density in the range from 0.5 to 10 W/cm^2, followed by a gentle roll off with increasing power density, reaching 1% at 1 kW/cm^2. These values are comparable to those achieved by the TFSI-treated samples[19] with PLQY reaching 3% at 10 W/cm^2 and 1% at 100 W/cm^2. Furthermore, we find that the mid-gap defect states of MoS_2 are neutralized in the light-soaked samples. As determined by direct excitation as a function of photon energy, the mechanism for neutralization of defect states for different organic/TMO blends is governed by the polaron pair concentration optically generated at the organic/TMO interface and subsequent TMO radical formation at the MoS_2 monolayer. Importantly, the treated monolayers (MoS_2 and WS_2) are found to be stable in air, vacuum, and acetone environments over time.

Received: May 6, 2021
Accepted: July 23, 2021
Published: August 4, 2021

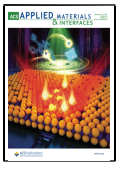

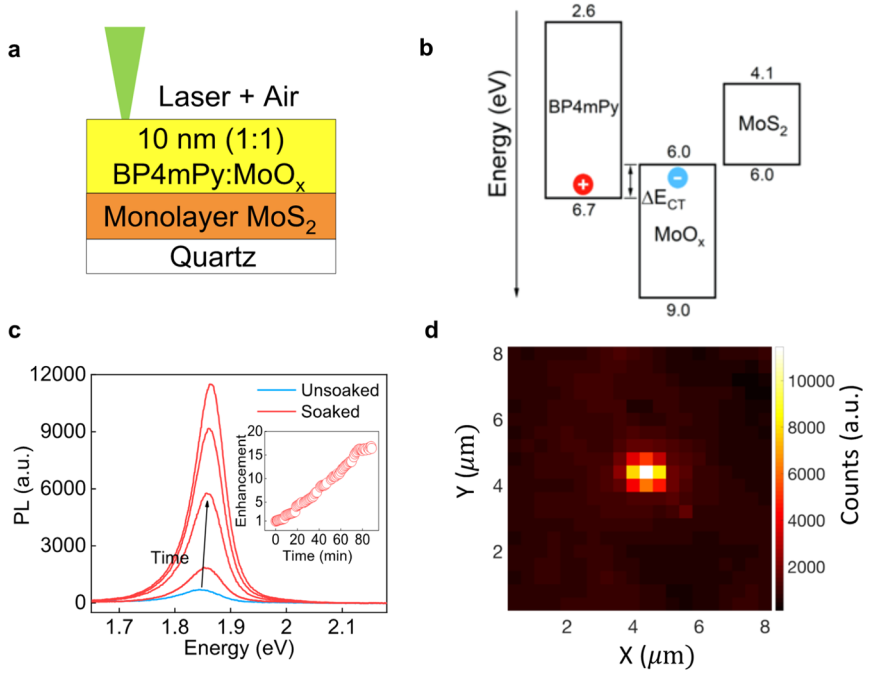

Figure 1. (a) Schematic of laser soaking in ambient with a 10 nm 1:1 (vol) BP4mPy/MoO_x blend on a MoS_2 monolayer. (b) Energy levels of BP4mPy, MoO_x, and MoS_2. The diagram also shows the negative polaron in MoO_x and the positive polaron in BP4mPy. (c) Steady-state PL spectra of MoS_2 over the course of laser soaking. Inset: evolution of the MoS_2 PL enhancement with soaking time compared to the as-exfoliated MoS_2 PL. (d) PL intensity map around a soaked spot.

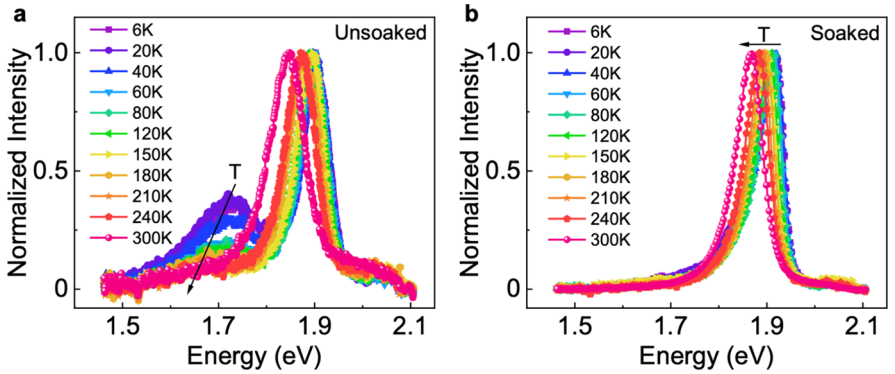

Figure 2. Normalized temperature-dependent PL spectra of MoS_2 (capped by 1:1 (vol) BP4mPy/MoO_x blend) (a) before and (b) after laser soaking. The arrow represents the spectral changes with increasing temperature.

RESULTS AND DISCUSSION

Figure 1a shows an illustration of a 10 nm 1:1 (vol) blend comprising BP4mPy/MoO_x that is vapor-deposited under high vacuum onto a mechanically exfoliated monolayer of MoS_2 on a quartz substrate. The BP4mPy and MoO_x molecules serve as electron donors and acceptors, respectively, and are transparent across the visible spectrum due to their wide energy gaps, as shown in Figure 1b. The sample is light-soaked in ambient by a continuous wave laser (photon energy = 2.3 eV and power density = 10^3 W/cm^2). Electrons in the highest occupied molecular orbital (HOMO) of BP4mPy are transferred to the conduction band (CB) of MoO_x, generating a Coulombically bound charge-transfer (CT) state. The CT state dissociates into free charged polarons via an intermediate precursor state often referred as a polaron pair. Simultaneously, excitons are created in the underlying MoS_2 monolayer, and the resulting PL is measured periodically during light soaking until no further enhancement in PL is observed. Figure 1c shows the evolution of PL intensity over 80 min of laser treatment. The PL peak shows a 16× enhancement and a ∼20 meV blue shift compared with the untreated sample. Figure 1d shows the PL map around a laser-soaked area. No significant change in PL is observed after storing the treated samples in ambient for 2 weeks (refer Supporting Information Figure S1), or after dipping in acetone for 30 min (refer Supporting Information Figure S9), indicating that the sample properties are passivated following this process. In addition, thermal annealing is ruled out as the driving mechanism for the neutralization process (refer to Figure S2 in the Supporting Information).

To understand the origin of the increased PL, the emission spectra of the unsoaked and soaked MoS_2 were acquired at temperatures varied between 6 and 300 K, with results shown in Figure 2a. Laser soaking was performed locally at room temperature before the sample temperature was changed. The spectra are taken from the same exfoliated MoS_2 monolayer

https://doi.org/10.1021/acsami.1c07956
ACS Appl. Mater. Interfaces 2021, 13, 44686−44692

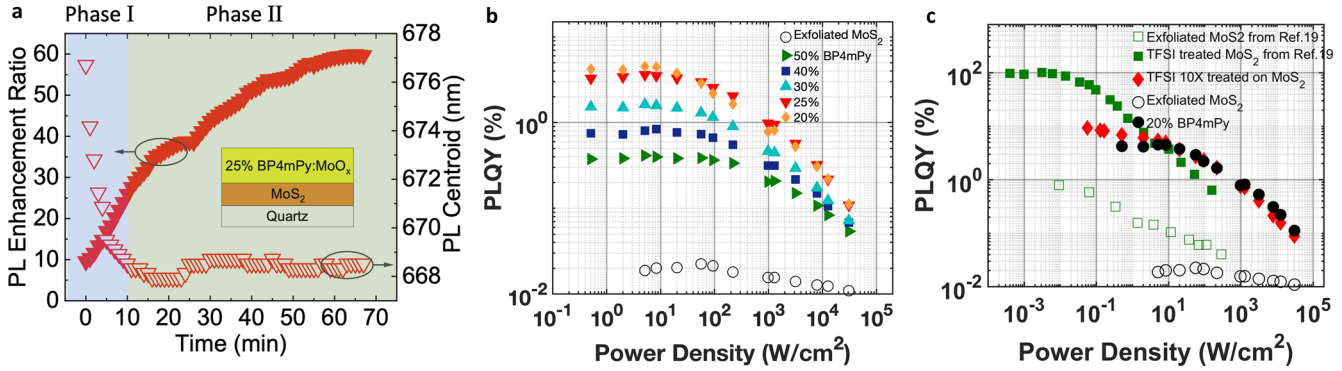

Figure 3. (a) Time evolution of PL enhancement and shift of the MoS_2 monolayer PL peak under laser soaking (10^3 W/cm^2) for the BP4mPy/MoO_x blend with the optimum ratio (BP4mPy (vol %) = 25%) compared to the as-exfoliated MoS_2 PL. (b) Pump-power-dependent PLQY of laser-soaked and as-exfoliated MoS_2 (error bars are smaller than the data symbols). (c) PLQY comparison of the laser-soaked sample with the TFSI-treated sample. The green squares are data-extracted from ref 19. Reprinted in part with permission from ref 19. Copyright 2015 American Association for the Advancement of Science.

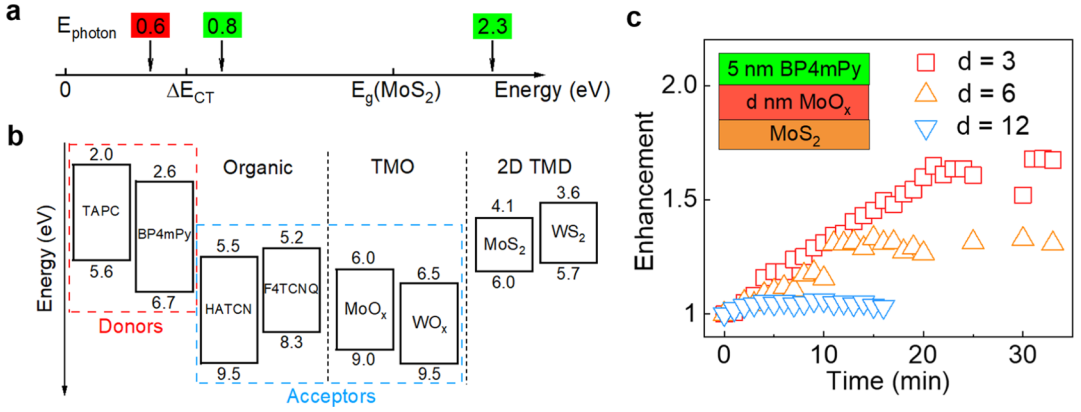

Figure 4. (a) Energies of the bound polaron pair (ΔE_{CT}) and band gap of MoS_2 (E_g) and of laser source (E_{photon}). Green (effective) and red (non-effective) labels indicate the effectiveness of PL enhancement, respectively. (b) Energy levels of TAPC, BP4mPy, HATCN, F4TCNQ, MoO_x, WO_x, MoS_2, and WS_2. (c) PL enhancement vs soaking time with passivation layer thickness, d (3, 6, and 12 nm) MoO_x capped by 5 nm BP4mPy. The laser energy is E_{photon} = 2.3 eV. Inset: Sample structure.

capped by the BP4mPy/MoO_x blend. The blend shows no emission from BP4mPy or MoO_x due to the low pump photon energy. In addition, broad mid-energy gap emission is observed at 1.7 eV, which has previously been attributed to crystallographic defect (sulfur vacancy) bound excitons.[13,15,32,36−38] The strong low-energy emission at 6 K suggests the existence of a large density of such defect states. In contrast, the laser-soaked sample in Figure 2b shows only band-edge excitons, suggesting that the mid-gap defect states are eliminated or neutralized. The narrowing of the full width at half-maximum of the PL after laser soaking indicates reduction in the inhomogeneous broadening arising from exciton defect scattering, further supporting the conclusion.

The temperature-dependent exciton peak energy of both unsoaked and soaked areas follow the Varshni equation[39] that characterizes temperature dependence of the semiconductor energy gap (refer the Supporting Information, Figure S3). We note that a ∼20 meV blue shift is observed between the spectra of soaked and unsoaked areas, suggesting a change of the free charge distribution of the inherently n-type MoS_2 monolayer that results in a transition of the dominant excited state species from charged (trions) to neutral excitons.[13,20,21,40,41] Since we observe reduction of intrinsic defect states accompanied by an increase in PL, we infer that the capping layers help to extract the excess charge,[13,20,32] while laser soaking neutralizes the mid-gap defect states.

We investigated the PL enhancement normalized to that of the as-exfoliated MoS_2 as a function of BP4mPy volume percentage in the BP4mPy/MoO_x blend ranging from 50 to 20%. An enhancement of ∼60× is observed for the 25% BP4mPy sample at a laser power of 1 kW/cm^2 as shown in Figure 3a. In comparison, the 50, 40, 30, and 20% samples yielded 16×, 29×, 40×, and 47× increases in PL intensity, respectively (refer Supporting Information Figure S4c). We note that a small, concentration-dependent enhancement was observed immediately before laser soaking—the MoO_x-rich blends resulted in higher enhancements. To understand the origin of this trend, we conducted the experiments with only one material layered onto MoS_2. The PL from MoS_2 increased by 3× after capping with neat MoO_x (refer Supporting Information Figure S4a). This enhancement is possibly due to very deep CB minimum of MoO_x relative to MoS_2 (refer Figure 1b) that results in a strong electron-withdrawing tendency (leading to a transition of dominant PL emission from trions to neutral excitons). In contrast, we observe a 5× decease in PL accompanied by a 16 meV red shift when capped only with BP4mPy, implying that the Fermi level of BP4mPy is higher than that of MoS_2, thereby acting as an electron donor. Hence, the MoO_x-rich blends lead to increased

https://doi.org/10.1021/acsami.1c07956
ACS Appl. Mater. Interfaces 2021, 13, 44686−44692

enhancement. Thus, the difference in PL enhancement after soaking is attributed to the different net charge concentration of MoS_2 provided by the various blends during soaking. We verified this by monitoring the blue shift in PL (refer Figure 3a), which follows the PL enhancement. In addition, we observed that the blue shift only occurs during the first 10 min of laser soaking (phase I). The continuous blue shift results due to charge extraction, possibly due to an increase of work function (i.e., a decrease of Fermi level) of MoO_x[42] from laser-induced oxidation.[43] No further shift in the MoS_2 peak was observed beyond phase I, although the PL continued to increase (soaking time >10 min, phase II), implying the termination of the charge extraction process, while neutralization of the intrinsic defect states continued.

Figure 3b shows the pump-power-dependent PLQY of a MoS_2 monolayer after laser-soaking for different capping blend ratios (refer Supporting Information Figure S5 for methods). In all cases, the PLQY increases dramatically with decreasing power density due to a decrease in nonradiative exciton−exciton Auger recombination, until saturating at ∼10 W/cm^2. Compared to the intrinsic PLQY = 0.018 ± 0.001% of as-exfoliated MoS_2, the 20%:80% BP4mPy/MoO_x blend yielded a maximum of 4.5 ± 0.2% at 10 W/cm^2 (∼250× PL enhancement) that decreased to 2.6 ± 0.1% at 10^2 W/cm^2. These values are comparable to TFSI-treated samples from ref 19 as shown in Figure 3c, where PLQY = 3% at 10 W/cm^2 and 1% at 10^2 W/cm^2. Figure 3c also includes data for exfoliated samples that were treated with TFSI in our lab. The values are comparable to those obtained from laser-soaked samples, albeit the defects are eliminated in the case of laser soaking.

We observed no PL enhancement after 3 h of soaking with a 0.6 eV (infrared) laser source (refer Figure 4a), whose energy is lower than the energy offset between the HOMO level of BP4mPY and the CB of MoO_x (ΔE_{CT} = 0.7 eV and refer Supporting Information Figure S6). In contrast, an intensity increase is observed immediately after soaking with 0.8 eV photons (refer Supporting Information Figure S6). This suggests that generation of CT states within the capping layer is necessary for the observed effect. However, the PL is found to decrease when MoO_x is replaced by the organic acceptor, 1,4,5,8,9,11-hexaazatriphenylenehexacarbonitrile (HAT-CN) or 2,3,5,6-tetrafluoro-7,7,8,8-tetracyanoquinodimethane (F4-TCNQ), that creates an organic/organic blend with a similar energy alignment as the BP4mPy/MoO_x blend (refer Figure 4b and Supporting Information Figure S7). In contrast, the PL responds to light soaking when MoO_x is replaced by WO_x (refer Supporting Information Figures S7 and S8 and Table S1). Hence, we conclude that TMO radicals formed following the dissociation of CT excitons play an essential role in the neutralization process. Indeed, light-soaking BP4mPy/MoO_x on MoS_2 in a N_2 atmosphere (O_2, H_2O < 1 ppm) does not result in PL enhancement. Furthermore, a heterobilayer structure comprising 5 nm BP4mPy/d nm MoO_x/MoS_2 was used to determine the effect of CT state formation as a function of distance d (varied from 3 to 12 nm) from the TMD (refer Figure 4c). In such a configuration, CTs are formed at the BP4mPy and MoO_x heterojunction and must diffuse across the MoO_x before reaching the MoS_2. The reduction in PL enhancement with increasing d results from the limited diffusion length of electrons formed following CT dissociation. This shows that the morphology between the immiscible components is critical for the process.

These results suggest a two-phase neutralization process described by the model in Figure 5. The photogenerated CT

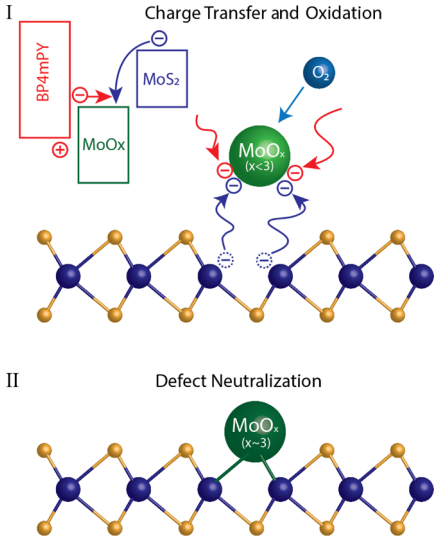

Figure 5. Schematic of the passivation process. The top panel shows phase I that is dominated by CT. The bottom panel (phase II) portrays the defect neutralization by the MoO_x radical.

states in the organic/TMO blend dissociate into free polarons via an intermediate polaron pair. The electron in MoO_x diffuses to the MoS_2 surface. Laser excitation creates MoO_x (or other TMO) radicals that bond to sulfur vacancy sites, neutralizing the reduced MoS_2 surface due to CT from MoO_x. Phase II is consistent with the reported work by Barja et al.,[45] where passivation of the selenide vacancies and elimination of the mid-gap defect states are achieved via oxygen exposure. The insertion of TMO radicals at the sulfur vacancies is also supported by the observed shift and narrowing of the Raman peaks (refer Supporting Information Figure S10). Furthermore, the intensity of the LA(M) peak (∼225 cm^{-1}) is proportional to the density of defects,[44] and we observe a decreasing trend, confirming the neutralization of the defect states (refer Supporting Information Figure S11). To further test this model, we substituted an inherently p-doped exfoliated WSe_2 monolayer for MoS_2. As expected, no PL enhancement was observed. We note that MoO_x has previously been observed to function as a photocatalyst. Hence, defect neutralization is also possible via formation of an oxygen radical ($O_2^{\bullet-}$). However, this is unlikely since we observe that the defect neutralization process is reversed upon rinsing the sample with a strong polar solvent such as water, since MoO_x dissolves in water (refer Supporting Information Figure S9).

CONCLUSIONS

Using laser soaking of organic/TMO blends, we confirmed the neutralization of mid-gap defect states in monolayer TMDs by low-temperature PL as shown in Figure 2. In this work, we use direct excitation as a function of photon energy to reveal the mechanism for neutralization of defect states for different organic/TMO blends. We find that the neutralization process is governed by the polaron pair concentration optically generated at the organic/TMO interface, and subsequent TMO radical formation at the MoS_2 monolayer. The intrinsic defect states in MoS_2 that lead to non-radiative exciton recombination are eliminated after treatment, leading to ∼250

https://doi.org/10.1021/acsami.1c07956
ACS Appl. Mater. Interfaces 2021, 13, 44686−44692

times enhancement in PLQY, increasing from 0.018 to ~4.5%. We find that the negative TMO radicals play an important role in neutralizing the sulfur vacancy defects on MoS_2 monolayers. Our approach provides a potential route to achieve defect-free optoelectronic devices based on 2D materials and 2D/organic heterojunctions.

METHODS

Sample Fabrication. Monolayers of MoS_2, WS_2, and WSe_2 (from 2D semiconductors, HQ Graphene) were mechanically exfoliated from bulk crystals on quartz substrates.[46] The materials BP4mPy (LT-N862), TAPC (LT-N137), HAT-CN (LT-N221), F4-TCNQ (LT-E208), and CBP (LT-E409) were purchased from Lumtec. MoO_x and WO_x were purchased from Sigma-Aldrich. Organic and TMO thin films were deposited onto the substrates or MoS_2 in a vacuum thermal evaporator at a base pressure of less than 5×10^{-7} Torr with deposition rates between 0.05 and 1 Å s^{-1}. The film thickness was measured using variable-angle spectroscopic ellipsometry (HS-190, J.A. Woollam, Inc). A cover glass slide was bonded to the substrate with an ultraviolet-curable epoxy (OG159-2, Epoxy Technology, Inc.) in a glovebox (O_2, H_2O < 1 ppm) to seal the sample in N_2. The treatment procedure with bis(trifluoromethane)sulfonimide (TFSI)[19] is as follows: 20 mg of TFSI (Sigma-Aldrich) was dissolved in 10 mL of 1,2-dichloroethane (DCE) (Sigma-Aldrich) to prepare a 2 mg/mL solution. The solution is further diluted with DCE to prepare a 0.2 mg/mL TFSI solution. The exfoliated sample was then immersed in the 0.2 mg/mL solution in a tightly closed vial for 10 min on a hotplate (100 °C). The sample was then removed and blow-dried with nitrogen without rinsing and subsequently annealed at 100 °C for 5 min. This process is repeated to maximize the PLQY.

Optical Measurements. The sample was pumped using a 2.33 eV continuous-wave diode laser focused toward a diffraction-limited spot for all PL measurements. The PL signal was directed to a spectrometer (IsoPlane-320 from Princeton Instruments), dispersed by a diffraction grating (300 grooves per mm), and detected by a CCD camera (PIXIS: 400BR). The low-temperature measurements were performed in a He flow cryostat (AttoDRY800). The absorption spectra were collected using a calibrated PerkinElmer LAMBDA 1050 ultraviolet−visible spectrometer. The PLQY of the organic thin film (10% PQIr/CBP) for calibration was measured using an integrating sphere connected to two-channel optical paths. One channel was designated for the optical pump, whereas the other channel was for the sample emission, incorporating a long- and short-pass filter, respectively, with a band edge of 550 nm. An additional optical neutral density (ND) filter of OD (optical density) 4 was added in the optical pump channel to reduce the pump intensity for improved sample emission sensitivity. The PL quantum yield was obtained from the spectrum following the previous work as follows[47]

$$\eta_{PL} = \frac{\alpha \int_{samp.em.} \frac{\lambda}{hc} I(\lambda) d\lambda}{10^{OD} \alpha \int_{opt.pump} \frac{\lambda}{hc} [I(\lambda) - I'(\lambda)] d\lambda}$$

where OD is the optical density of the ND filter, α is the calibration factor for the measurement setup, λ is the wavelength, h is Planck's constant, c is the speed of light, $I(\lambda)$ is the PL spectrum with the sample present, and $I'(\lambda)$ is the PL spectrum of the excitation laser without the sample. The power-dependent PLQY of MoS_2 monolayers was achieved using a time-correlated single-photon counting module (HydraHarp 400) and a single-photon avalanche photodiode (Micro Photon Devices) and calibrated by the PLQY of the organic thin film. The supercontinuum laser is described in reference.[48] Raman spectra were collected using a Renishaw in Via Raman Microscopy system equipped with a 500 μW 532 nm continuous-wave laser, an 1800 lines/mm grating and a RenCam CCD detector.

ASSOCIATED CONTENT

Supporting Information

The Supporting Information is available free of charge at https://pubs.acs.org/doi/10.1021/acsami.1c07956.

Reliability; thermal effects; temperature-dependent PL; CT and neutralization; PLQY measurement; laser energy-dependent soaking; material-dependent laser soaking; laser soaking on WS_2; stability in solvents; in situ Raman spectroscopy; and table of effectiveness of laser soaking for different organic/TMO blends and TMDs (PDF)

AUTHOR INFORMATION

Corresponding Author

Parag B. Deotare − *Department of Electrical Engineering and Computer Science, University of Michigan, Ann Arbor, Michigan 48109, United States;* orcid.org/0000-0002-9867-7380; Email: pdeotare@umich.edu

Authors

Xiaheng Huang − *Department of Electrical Engineering and Computer Science, University of Michigan, Ann Arbor, Michigan 48109, United States*

Zidong Li − *Department of Electrical Engineering and Computer Science, University of Michigan, Ann Arbor, Michigan 48109, United States;* orcid.org/0000-0002-0984-9778

Xiao Liu − *Department of Electrical Engineering and Computer Science, University of Michigan, Ann Arbor, Michigan 48109, United States;* orcid.org/0000-0002-5397-6694

Jize Hou − *Department of Electrical Engineering and Computer Science, University of Michigan, Ann Arbor, Michigan 48109, United States*

Jongchan Kim − *Department of Electrical Engineering and Computer Science, University of Michigan, Ann Arbor, Michigan 48109, United States*

Stephen R. Forrest − *Department of Electrical Engineering and Computer Science, University of Michigan, Ann Arbor, Michigan 48109, United States; Department of Physics, University of Michigan, Ann Arbor, Michigan 48109, United States; Department of Materials Science and Engineering, University of Michigan, Ann Arbo, Michigan 48109, United States;* orcid.org/0000-0003-0131-1903

Complete contact information is available at: https://pubs.acs.org/10.1021/acsami.1c07956

Author Contributions

‖X.H. and Z.L. contributed equally to this work.

Notes

The authors declare no competing financial interest.

ACKNOWLEDGMENTS

S.R.F. thanks the Army Research Office (contract W911NF-17-1-0312) for partial support of this work. P.B.D. acknowledges the support of Air Force Office of Scientific Research (AFOSR) award no. FA9550-17-1-0208. The authors acknowledge Kaiwen Guo, Tianqu Zhai, and Mohammed N Islam for their help with the supercontinuum laser.

REFERENCES

(1) Shim, J.; Bae, S.-H.; Kong, W.; Lee, D.; Qiao, K.; Nezich, D.; Park, Y. J.; Zhao, R.; Sundaram, S.; Li, X.; Yeon, H.; Choi, C.; Kum, H.; Yue, R.; Zhou, G.; Ou, Y.; Lee, K.; Moodera, J.; Zhao, X.; Ahn, J.-H.; Hinkle, C.; Ougazzaden, A.; Kim, J. Controlled Crack Propagation for Atomic Precision Handling of Wafer-Scale Two-Dimensional Materials. *Science* **2018**, *362*, 665−670.

(2) Bae, S.-H.; Kum, H.; Kong, W.; Kim, Y.; Choi, C.; Lee, B.; Lin, P.; Park, Y.; Kim, J. Integration of Bulk Materials with Two-Dimensional Materials for Physical Coupling and Applications. *Nat. Mater.* **2019**, *18*, 550−560.

(3) Kang, K.; Xie, S.; Huang, L.; Han, Y.; Huang, P. Y.; Mak, K. F.; Kim, C.-J.; Muller, D.; Park, J. High-Mobility Three-Atom-Thick Semiconducting Films with Wafer-Scale Homogeneity. *Nature* **2015**, *520*, 656−660.

(4) Wang, Q.; Li, N.; Tang, J.; Zhu, J.; Zhang, Q.; Jia, Q.; Lu, Y.; Wei, Z.; Yu, H.; Zhao, Y.; Guo, Y.; Gu, L.; Sun, G.; Yang, W.; Yang, R.; Shi, D.; Zhang, G. Wafer-Scale Highly Oriented Monolayer MoS 2 with Large Domain Sizes. *Nano Lett.* **2020**, *20*, 7193.

(5) Liu, X.; Gu, J.; Ding, K.; Fan, D.; Hu, X.; Tseng, Y.-W.; Lee, Y.-H.; Menon, V.; Forrest, S. R. Photoresponse of an Organic Semiconductor/Two-Dimensional Transition Metal Dichalcogenide Heterojunction. *Nano Lett.* **2017**, *17*, 3176−3181.

(6) Gu, J.; Chakraborty, B.; Khatoniar, M.; Menon, V. M. A Room-Temperature Polariton Light-Emitting Diode Based on Monolayer WS2. *Nat. Nanotechnol.* **2019**, *14*, 1024−1028.

(7) Cho, J.; Amani, M.; Lien, D. H.; Kim, H.; Yeh, M.; Wang, V.; Tan, C.; Javey, A. Centimeter-Scale and Visible Wavelength Monolayer Light-Emitting Devices. *Adv. Funct. Mater.* **2019**, *30*, 1907941.

(8) Lim, Y. R.; Song, W.; Han, J. K.; Lee, Y. B.; Kim, S. J.; Myung, S.; Lee, S. S.; An, K.-S.; Choi, C.-J.; Lim, J. Wafer-Scale, Homogeneous MoS2Layers on Plastic Substrates for Flexible Visible-Light Photodetectors. *Adv. Mater.* **2016**, *28*, 5025−5030.

(9) Pospischil, A.; Furchi, M. M.; Mueller, T. Solar-Energy Conversion and Light Emission in an Atomic Monolayer p−n Diode. *Nat. Nanotechnol.* **2014**, *9*, 257−261.

(10) Ross, J. S.; Klement, P.; Jones, A. M.; Ghimire, N. J.; Yan, J.; Mandrus, D. G.; Taniguchi, T.; Watanabe, K.; Kitamura, K.; Yao, W.; Cobden, D. H.; Xu, X. Electrically Tunable Excitonic Light-Emitting Diodes Based on Monolayer WSe2 p-n Junctions. *Nat. Nanotechnol.* **2014**, *9*, 268−272.

(11) Li, N.; Wang, Q.; Shen, C.; Wei, Z.; Yu, H.; Zhao, J.; Lu, X.; Wang, G.; He, C.; Xie, L.; Zhu, J.; Du, L.; Yang, R.; Shi, D.; Zhang, G. Large-Scale Flexible and Transparent Electronics Based on Monolayer Molybdenum Disulfide Field-Effect Transistors. *Nat. Electron.* **2020**, *3*, 711.

(12) Hong, J.; Hu, Z.; Probert, M.; Li, K.; Lv, D.; Yang, X.; Gu, L.; Mao, N.; Feng, Q.; Xie, L.; Zhang, J.; Wu, D.; Zhang, Z.; Jin, C.; Ji, W.; Zhang, X.; Yuan, J.; Zhang, Z. Exploring Atomic Defects in Molybdenum Disulphide Monolayers. *Nat. Commun.* **2015**, *6*, 6293.

(13) Greben, K.; Arora, S.; Harats, M. G.; Bolotin, K. I. Intrinsic and Extrinsic Defect-Related Excitons in TMDCs. *Nano Lett.* **2020**, *20*, 2544−2550.

(14) Zhou, W.; Zou, X.; Najmaei, S.; Liu, Z.; Shi, Y.; Kong, J.; Lou, J.; Ajayan, P. M.; Yakobson, B. I.; Idrobo, J.-C. Intrinsic Structural Defects in Monolayer Molybdenum Disulfide. *Nano Lett.* **2013**, *13*, 2615−2622.

(15) Komsa, H. P.; Krasheninnikov, A. V. Native Defects in Bulk and Monolayer MoS2 from First Principles. *Phys. Rev. B: Condens. Matter Mater. Phys.* **2015**, *91*, 125304.

(16) Cadiz, F.; Courtade, E.; Robert, C.; Wang, G.; Shen, Y.; Cai, H.; Taniguchi, T.; Watanabe, K.; Carrere, H.; Lagarde, D.; Manca, M.; Amand, T.; Renucci, P.; Tongay, S.; Marie, X.; Urbaszek, B. Excitonic Linewidth Approaching the Homogeneous Limit in MoS2-Based van Der Waals Heterostructures. *Phys. Rev. X* **2017**, *7*, 021026.

(17) Rhodes, D.; Chae, S. H.; Ribeiro-Palau, R.; Hone, J. Disorder in van Der Waals Heterostructures of 2D Materials. *Nat. Mater.* **2019**, *18*, 541−549.

(18) Mak, K. F.; Lee, C.; Hone, J.; Shan, J.; Heinz, T. F. Atomically Thin MoS2: A New Direct-Gap Semiconductor. *Phys. Rev. Lett.* **2010**, *105*, 136805.

(19) Amani, M.; Lien, D.-H.; Kiriya, D.; Xiao, J.; Azcatl, A.; Noh, J.; Madhvapathy, S. R.; Addou, R.; Kc, S.; Dubey, M.; Cho, K.; Wallace, R. M.; Lee, S.-C.; He, J.-H.; Ager, J. W.; Zhang, X.; Yablonovitch, E.; Javey, A. Near-Unity Photoluminescence Quantum Yield in MoS2. *Science* **2015**, *350*, 1065−1068.

(20) Lien, D.-H.; Uddin, S. Z.; Yeh, M.; Amani, M.; Kim, H.; Ager, J. W.; Yablonovitch, E.; Javey, A. Electrical Suppression of All Nonradiative Recombination Pathways in Monolayer Semiconductors. *Science* **2019**, *364*, 468−471.

(21) Mouri, S.; Miyauchi, Y.; Matsuda, K. Tunable Photoluminescence of Monolayer MoS2 via Chemical Doping. *Nano Lett.* **2013**, *13*, 5944−5948.

(22) Peimyoo, N.; Yang, W.; Shang, J.; Shen, X.; Wang, Y.; Yu, T. Chemically Driven Tunable Light Emission of Charged and Neutral Excitons in Monolayer WS2. *ACS Nano* **2014**, *8*, 11320−11329.

(23) Tongay, S.; Zhou, J.; Ataca, C.; Liu, J.; Kang, J. S.; Matthews, T. S.; You, L.; Li, J.; Grossman, J. C.; Wu, J. Broad-Range Modulation of Light Emission in Two-Dimensional Semiconductors by Molecular Physisorption Gating. *Nano Lett.* **2013**, *13*, 2831−2836.

(24) Tanoh, A. O. A.; Alexander-Webber, J.; Xiao, J.; Delport, G.; Williams, C. A.; Bretscher, H.; Gauriot, N.; Allardice, J.; Pandya, R.; Fan, Y.; Li, Z.; Vignolini, S.; Stranks, S. D.; Hofmann, S.; Rao, A. Enhancing Photoluminescence and Mobilities in WS2 Monolayers with Oleic Acid Ligands. *Nano Lett.* **2019**, *19*, 6299−6307.

(25) Park, J. H.; Sanne, A.; Guo, Y.; Amani, M.; Zhang, K.; Movva, H. C. P.; Robinson, J. A.; Javey, A.; Robertson, J.; Banerjee, S. K.; Kummel, A. C. Defect Passivation of Transition Metal Dichalcogenides via a Charge Transfer van Der Waals Interface. *Sci. Adv.* **2017**, *3*, 1701661.

(26) Zheng, B.; Zheng, W.; Jiang, Y.; Chen, S.; Li, D.; Ma, C.; Wang, X.; Huang, W.; Zhang, X.; Liu, H.; Jiang, F.; Li, L.; Zhuang, X.; Wang, X.; Pan, A. WO3-WS2 Vertical Bilayer Heterostructures with High Photoluminescence Quantum Yield. *J. Am. Chem. Soc.* **2019**, *141*, 11754−11758.

(27) Han, H.-V.; Lu, A.-Y.; Lu, L.-S.; Huang, J.-K.; Li, H.; Hsu, C.-L.; Lin, Y.-C.; Chiu, M.-H.; Suenaga, K.; Chu, C.-W.; Kuo, H.-C.; Chang, W.-H.; Li, L.-J.; Shi, Y. Photoluminescence Enhancement and Structure Repairing of Monolayer MoSe2 by Hydrohalic Acid Treatment. *ACS Nano* **2016**, *10*, 1454−1461.

(28) Wang, W.; Shu, H.; Wang, J.; Cheng, Y.; Liang, P.; Chen, X. Defect Passivation and Photoluminescence Enhancement of Monolayer MoS2 Crystals through Sodium Halide-Assisted Chemical Vapor Deposition Growth. *ACS Appl. Mater. Interfaces* **2020**, *12*, 9563−9571.

(29) Huo, N.; Huang, L.; Shu, K.; Yang, M.; Luo, D.; Li, J. Improved Photoluminescence in 2D Semiconductors Induced by Interface Magnetization. *ACS Photonics* **2020**, *7*, 3341−3345.

(30) Neupane, G. P.; Tran, M. D.; Yun, S. J.; Kim, H.; Seo, C.; Lee, J.; Han, G. H.; Sood, A. K.; Kim, J. Simple Chemical Treatment to N-Dope Transition-Metal Dichalcogenides and Enhance the Optical and Electrical Characteristics. *ACS Appl. Mater. Interfaces* **2017**, *9*, 11950−11958.

(31) Yao, H.; Liu, L.; Wang, Z.; Li, H.; Chen, L.; Pam, M. E.; Chen, W.; Yang, H. Y.; Zhang, W.; Shi, Y. Significant Photoluminescence Enhancement in WS2 Monolayers through Na2S Treatment. *Nanoscale* **2018**, *10*, 6105−6112.

(32) Goodman, A. J.; Willard, A. P.; Tisdale, W. A. Exciton Trapping Is Responsible for the Long Apparent Lifetime in Acid-Treated MoS2. *Phys. Rev. B* **2017**, *96*, 121404.

(33) Sivaram, S. V.; Hanbicki, A. T.; Rosenberger, M. R.; Jernigan, G. G.; Chuang, H.-J.; McCreary, K. M.; Jonker, B. T. Spatially Selective Enhancement of Photoluminescence in MoS 2 by Exciton-Mediated Adsorption and Defect Passivation. *ACS Appl. Mater. Interfaces* **2019**, *11*, 16147−16155.

(34) Ardekani, H.; Younts, R.; Yu, Y.; Cao, L.; Gundogdu, K. Reversible Photoluminescence Tuning by Defect Passivation via Laser

https://doi.org/10.1021/acsami.1c07956
ACS Appl. Mater. Interfaces 2021, 13, 44686−44692

Irradiation on Aged Monolayer MoS2. *ACS Appl. Mater. Interfaces* **2019**, *11*, 38240−38246.
(35) Nan, H.; Wang, Z.; Wang, W.; Liang, Z.; Lu, Y.; Chen, Q.; He, D.; Tan, P.; Miao, F.; Wang, X.; Wang, J.; Ni, Z. Strong Photoluminescence Enhancement of MoS2 through Defect Engineering and Oxygen Bonding. *ACS Nano* **2014**, *8*, 5738−5745.
(36) Chow, P. K.; Jacobs-Gedrim, R. B.; Gao, J.; Lu, T.-M.; Yu, B.; Terrones, H.; Koratkar, N. Defect-Induced Photoluminescence in Monolayer Semiconducting Transition Metal Dichalcogenides. *ACS Nano* **2015**, *9*, 1520−1527.
(37) Tongay, S.; Suh, J.; Ataca, C.; Fan, W.; Luce, A.; Kang, J. S.; Liu, J.; Ko, C.; Raghunathanan, R.; Zhou, J.; Ogletree, F.; Li, J.; Grossman, J. C.; Wu, J. Defects Activated Photoluminescence in Two-Dimensional Semiconductors: Interplay between Bound, Charged, and Free Excitons. *Sci. Rep.* **2013**, *3*, 2657.
(38) Refaely-Abramson, S.; Qiu, D. Y.; Louie, S. G.; Neaton, J. B. Defect-Induced Modification of Low-Lying Excitons and Valley Selectivity in Monolayer Transition Metal Dichalcogenides. *Phys. Rev. Lett.* **2018**, *121*, 167402.
(39) Varshni, Y. P. Temperature Dependence of the Energy Gap in Semiconductors. *Physica* **1967**, *34*, 149−154.
(40) Mak, K. F.; He, K.; Lee, C.; Lee, G. H.; Hone, J.; Heinz, T. F.; Shan, J. Tightly Bound Trions in Monolayer MoS 2. *Nat. Mater.* **2013**, *12*, 207−211.
(41) Radisavljevic, B.; Radenovic, A.; Brivio, J.; Giacometti, V.; Kis, A. Single-Layer MoS2 Transistors. *Nat. Nanotechnol.* **2011**, *6*, 147−150.
(42) Greiner, M. T.; Chai, L.; Helander, M. G.; Tang, W.-M.; Lu, Z.-H. Transition Metal Oxide Work Functions: The Influence of Cation Oxidation State and Oxygen Vacancies. *Adv. Funct. Mater.* **2012**, *22*, 4557−4568.
(43) Cuando-Espitia, N.; Redenius, J.; Mensink, K.; Camacho-López, M.; Camacho-López, S.; Aguilar, G. Influence of Oxygen Pressure on the Fs Laser-Induced Oxidation of Molybdenum Thin Films. *Opt. Mater. Express* **2018**, *8*, 581.
(44) Mignuzzi, S.; Pollard, A. J.; Bonini, N.; Brennan, B.; Gilmore, I. S.; Pimenta, M. A.; Richards, D.; Roy, D. Effect of Disorder on Raman Scattering of Single-Layer Mo S2. *Phys. Rev. B: Condens. Matter Mater. Phys.* **2015**, *91*, 195411.
(45) Barja, S.; Refaely-Abramson, S.; Schuler, B.; Qiu, D. Y.; Pulkin, A.; Wickenburg, S.; Ryu, H.; Ugeda, M. M.; Kastl, C.; Chen, C.; Hwang, C.; Schwartzberg, A.; Aloni, S.; Mo, S. K.; Frank Ogletree, D.; Crommie, M. F.; Yazyev, O. V.; Louie, S. G.; Neaton, J. B.; Weber-Bargioni, A. Identifying Substitutional Oxygen as a Prolific Point Defect in Monolayer Transition Metal Dichalcogenides. *Nat. Commun.* **2019**, *10*, 3382.
(46) Li, Z.; Lu, X.; Cordovilla Leon, D. F.; Lyu, Z.; Xie, H.; Hou, J.; Lu, Y.; Guo, X.; Kaczmarek, A.; Taniguchi, T.; Watanabe, K.; Zhao, L.; Yang, L.; Deotare, P. B. Interlayer Exciton Transport in MoSe2/WSe2Heterostructures. *ACS Nano* **2021**, *15*, 1539.
(47) Kawamura, Y.; Sasabe, H.; Adachi, C. Simple Accurate System for Measuring Absolute Photoluminescence Quantum Efficiency in Organic Solid-State Thin Films. *Jpn. J. Appl. Phys., Part 1* **2004**, *43*, 7729−7730.
(48) Guo, K.; Zhai, T.; Demory, B.; Meah, S.; Martinez, R. A.; Islam, M. N.; Terry, F.; Maynard, R. Stand-off Non-Destructive Determination of Protein Level in Wheat Flour with a Super-Continuum Laser. *Optical Biopsy XVIII: Toward Real-Time Spectroscopic Imaging and Diagnosis*, 2020.

https://doi.org/10.1021/acsami.1c07956
ACS Appl. Mater. Interfaces 2021, 13, 44686−44692